



## Mapping sky, tree, and building view factors of street canyons in a high-density urban environment



Fang-Ying Gong<sup>a,b,\*</sup>, Zhao-Cheng Zeng<sup>c</sup>, Fan Zhang<sup>d</sup>, Xiaojiang Li<sup>e</sup>, Edward Ng<sup>a,f,g</sup>, Leslie K. Norford<sup>b</sup>

<sup>a</sup> School of Architecture, The Chinese University of Hong Kong, Shatin NT, Hong Kong

<sup>b</sup> Department of Architecture, Massachusetts Institute of Technology, Cambridge, MA, USA

<sup>c</sup> Division of Geological and Planetary Sciences, California Institute of Technology, Pasadena, CA, USA

<sup>d</sup> Institute of Space and Earth Information Science, The Chinese University of Hong Kong, Shatin NT, Hong Kong

<sup>e</sup> Senseable City Laboratory, Massachusetts Institute of Technology, Cambridge, MA, USA

<sup>f</sup> Institute of Environment, Energy and Sustainability, The Chinese University of Hong Kong, Shatin NT, Hong Kong

<sup>g</sup> Institute of Future Cities, The Chinese University of Hong Kong, Shatin NT, Hong Kong

### ARTICLE INFO

#### Keywords:

View factor  
Google Street View  
Deep learning  
Street trees  
Street canyon  
High density

### ABSTRACT

View factors for sky, trees, and buildings are three important parameters of the urban outdoor environment that describe the geometrical relationship between different surfaces from the perspective of radiative energy transfer. This study develops an approach for accurately estimating sky view factor (SVF), tree view factor (TVF), and building view factor (BVF) of street canyons in the high-density urban environment of Hong Kong using publicly available Google Street View (GSV) images and a deep-learning algorithm for extraction of street features (sky, trees, and buildings). As a result, SVF, TVF, and BVF maps of street canyons are generated. Verification using reference data of hemispheric photography from field surveys in compact high-rise and low-rise areas shows that the GSV-based VF estimates have a satisfying agreement with the reference data (all with  $R^2 > 0.95$ ), suggesting the effectiveness and high accuracy of the developed method. This is the first reported use of hemispheric photography for direct verification in a GSV-based streetscape study. Furthermore, a comparison between GSV-based and 3D-GIS-based SVFs shows that the two SVF estimates are significantly correlated ( $R^2 = 0.40$ ,  $p < 0.01$ ) and show better agreement in high-density areas. However, the latter overestimates SVF by 0.11 on average, and the differences between them are significantly correlated with street trees ( $R^2 = 0.53$ ): the more street trees, the larger the difference. This suggests that a lack of street trees in a 3D-GIS model of street environments is the dominant factor contributing to the large discrepancies between the two datasets.

### 1. Introduction

The urban thermal environment has practical implications for energy consumption, human comfort and productivity, air pollution at the street level, and urban ecology [1,2]. It is influenced by the geometry of street canyons, street trees, building blocks and impervious ground covers [3]. Street view factors (VFs) for the sky, trees, and buildings are three important parameters of urban outdoor environments. They describe the geometrical relation between different urban street components from the perspective of radiative energy transfer that plays a key role in urban thermal environments. Sky view factor (SVF), tree view factor (TVF), and building view factor (BVF) are defined as the geometric ratio of the amount of the sky, trees, and buildings seen, respectively, from a given surface point to the overlying hemisphere

subtended by a horizontal surface [4,5]. A thorough quantification and understanding of the physical streetscape using VFs, including its features and dynamics, offers great utility to urban planners and climatologists investigating the urban environment, its physical and social interactions, and implications for human well-being.

SVF, a geometric quantification of the degree of sky visibility within street canyons, is a commonly used indicator for describing urban geometry. As an effective indicator of nocturnal urban radiation balance, SVF characterizes the ratio of received (or emitted) radiation by an urban street to the total radiation emitted (or received) by the entire hemispheric radiation environment [6]. Therefore, SVF is an important geometrical parameter for the studies of urban microclimate [7,8], nocturnal urban heat island (UHI) effect [9,10], urban thermal comfort [7–11], and urban air pollution [12]. Street tree canopy, quantified by

\* Corresponding author. Rm505, AIT Building, School of Architecture, The Chinese University of Hong Kong, Shatin NT, Hong Kong.  
E-mail addresses: [fangying@link.cuhk.edu.hk](mailto:fangying@link.cuhk.edu.hk), [gongfy@mit.edu](mailto:gongfy@mit.edu) (F.-Y. Gong).

Nomenclature	
<i>Symbols and abbreviations</i>	
3D-GIS	Three-dimension geographic information system
API	Application programming interface
BVF	Building view factor
CNN	Convolutional neural network
DSM	Digital surface model
FCN	Fully convolutional network
GSV	Google Street View
H/W	Building-height-to-street-width
PSPNet	Pyramid scene parsing network
RMSE	Root-mean-square error
SVF	Sky view factor
TVF	Tree view factor
UHI	Urban heat island
URL	Uniform resource locator
VF	View factor
$x_p, y_p$	Coordinates of the cylindrical panorama
$x_f, y_f$	Coordinates of the fisheye image
$C_x, C_y$	Coordinates of the center pixel on the fisheye image
$H_p$	Height of the panorama image
$W_p$	Width of the panorama image
$R^2$	Coefficient of determination
$\alpha_{i, x}$	Angular width of pixels of feature $x$ ( $x$ can be sky, tree, or building) in the $i$ th ring
$\Psi_x$	View factor for sky, tree, and building when $x$ is specified
$r_0$	Radius of the fisheye image

TVF, has instrumental ecological service functions such as UHI mitigation due to its contribution to reducing urban temperature [13–16]. The trees' cooling effect comes from tree shading, which reduces the radiation reaching ground level [17,18], and evaporative cooling from leaf surfaces [19]. In addition, urban street trees have been found to absorb airborne pollution and therefore decrease road traffic emissions [20] and improve the walkability of streets [21]. Therefore, the proportion of street tree cover can be used to evaluate the benefits from ecosystem service provisions in different areas of a city [22]. Many urban materials for buildings have a relatively high heat capacity and surface thermal admittance, which make them efficiently accept and retain heat during daytime and release it at night, leading to a strong UHI effect [23,24]. This study uses BVF to quantify the impact of buildings on the urban radiative balance. These three VFs interact with each other in balancing urban radiation. SVF is a combination factor of buildings and trees that influences the air temperature [25]. Street trees reduce SVF by providing shading to the environment, resulting in the reduction of nighttime net longwave loss [26]. Buildings emit a greater amount of longwave radiation compared to the cool sky and trees [27]. Therefore, urban street canyons with a higher BVF will yield a larger net longwave radiation.

Methods for estimating VFs of urban street canyons can be grouped into the following three types:

1) Photographic method. This method uses a fish-eye lens to take on-site photographs that project the hemispheric environment onto a circular plane. Different street features are then extracted from the fisheye image to calculate the VFs. This method provides a direct

and accurate measurement of SVF [28,29]. However, taking on-site fisheye images usually requires fieldwork that is time- and effort-consuming. Therefore, this method is suitable only for small-scale study;

- 2) Model simulation. This method can produce spatially continuous VFs based on vectored buildings and rasterized digital 3D surface models [30–33]. However, model data are difficult to accurately generate and are therefore not always available. The accuracy of VF estimations using model simulations depends heavily on the accuracy of the model in simulating the street environment. However, the street environment can be very complex, such as those in the high-density urban areas of Hong Kong. In particular, the street tree canopy, a major component of streetscapes, is hard to parameterize in models;
- 3) Street-sensing method based on street-view panoramas. This recently proposed concept uses publicly and freely accessible street panoramic photographs, e.g. Google Street View (GSV) images, to derive VFs of street canyons by projecting the panorama into fisheye images [34–37]. Since GSV images directly capture urban streetscape and are available in many cities all over the world, this method provides a low cost and effective streetscape mapping approach for urban studies.

Li et al. [34] showed two examples demonstrating the usage of GSV images in mapping street tree and openness, while Liang et al. [35] provided a proof-of-concept study to show the reliability of using street panorama images in estimating SVF. Carrasco-Hernandez et al. (2015) proposed using the GSV images to calculate the street-level total

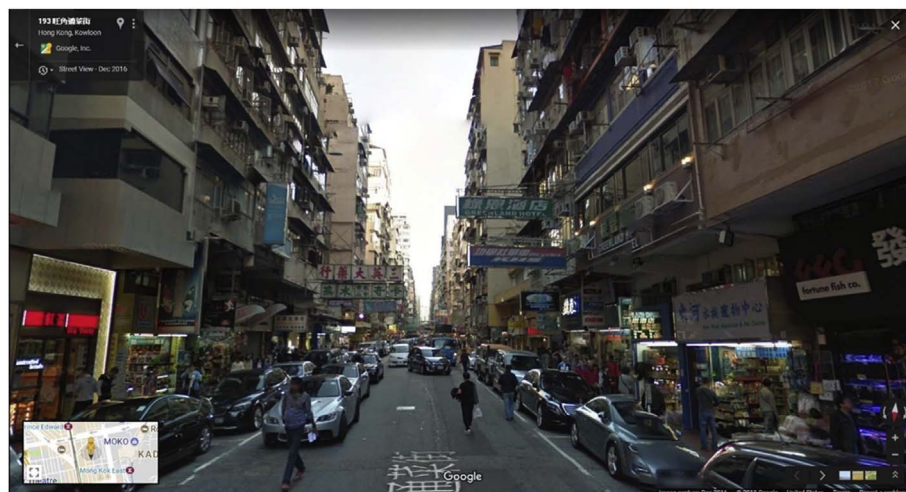


Fig. 1. An example of the deep street canyon in the Mong Kok area (shown in Fig. 2), one of the typical high-density high-rise urban areas of Hong Kong. (Source: GSV, 2016).

shortwave irradiance based on urban canyon geometries estimated from an open-source panorama generating tool [36]. Middel et al. (2017) used GSV-estimated SVF to verify the synthetic hemispherical fisheye photos at fine spatial resolution generated from a developed web-based tool using Google Earth 3D data for urban areas [37].

However, the previous study areas mainly focus on the cities where streetscape features are relatively simple (compared to high-density urban areas of Hong Kong in this paper) with well-defined building and street structures. The feasibility and uncertainty of using GSV for estimating SVF in such high-density context, are still not clear. Hong Kong, located in monsoon Asia, has a high-rise, high-density, and compact urban morphology with high building-height-to-street-width (H/W) ratio [38]. A typical street in high-density urban areas of Hong Kong is characterized by high-rise buildings, narrow compacted streets, interferences of heavy travel volume and pedestrian flow, and complex streetscapes with the amount of colorful overhanging signboards that block sunlight and air paths and provide limited openness to the sky (see Fig. 1). An effective and accurate method for mapping the VFs of the street canyons in Hong Kong is therefore crucial for studying its urban climate and assessing the relevant outdoor thermal comfort.

The purpose of this study is to develop an approach for estimating and mapping SVF, TVF, and BVF of street canyons in complex urban living environments, such as the high-density urban areas of Hong Kong. The approach is based on GSV images and a deep-learning technique for street feature extraction and is verified using hemispheric photography measurements as reference data from fieldwork. This verification is, to our knowledge, the first reported use of hemispheric photography for direct verification of GSV-based streetscape study. The developed approach represents a ground-based perspective of city streetscapes that cover complicated urban contexts, including tree canopy cover, building overhangs, and shade structures. A comparison with conventional 3D modeling of SVF, which has been widely used in previous studies, is also conducted to assess the uncertainty and advantages of this GSV-based mapping approach.

## 2. Methods

### 2.1. Study area

Hong Kong, situated on the coastline of southeastern China (see Fig. 2), is one of the most densely-populated and built-up cities in the world. It has a population of over seven million living in around 262 km<sup>2</sup> of developed land [39,40]. The climate of Hong Kong is subtropical maritime, which features hot and humid summers and warm winters [41]. Moreover, high-density urban areas of Hong Kong are characterized by high-rise compact building blocks and deep street canyons with a high H/W ratio. In these areas, tall buildings of some 40-60 stories lining narrow streets of 15–25 m width have been the norm. Serious issues related to human thermal comfort [42], air pollution [43] and the UHI effect [44] due to its climate and urban morphologies have been primary planning concerns. As effective indicators for characterizing urban streetscapes, street VFs have been widely incorporated in modeling to address these concerns. However, an assessment of the accuracy of VF estimations, which is crucial for quantifying the uncertainty of models, is still lacking due to a lack of measurements.

In this study, high-density urban regions of Kowloon and Hong Kong Island are chosen as our study area, as shown in Fig. 2. This area is one of the most densely built and populated areas in the world, with a mean building height of 27 m, a standard deviation of 30.7 m, and a population density of around 42,900 persons per km<sup>2</sup>. As shown in Fig. 2 (c), the building heights are grouped into high-rise (> 25 m), mid-rise (15–25 m) and low-rise (< 15 m), according to local climate zone classification in Hong Kong urban areas [45,46]. Most high-rise buildings are distributed in southern Kowloon and northern Hong Kong Island.

### 2.2. GSV-based SVF, TVF and BVF estimates

In this study, we use publicly accessible GSV images to estimate the SVF, TVF, and BVF of street canyons in high-density urban areas of Hong Kong. Street panorama images sampled at 30 m intervals are first

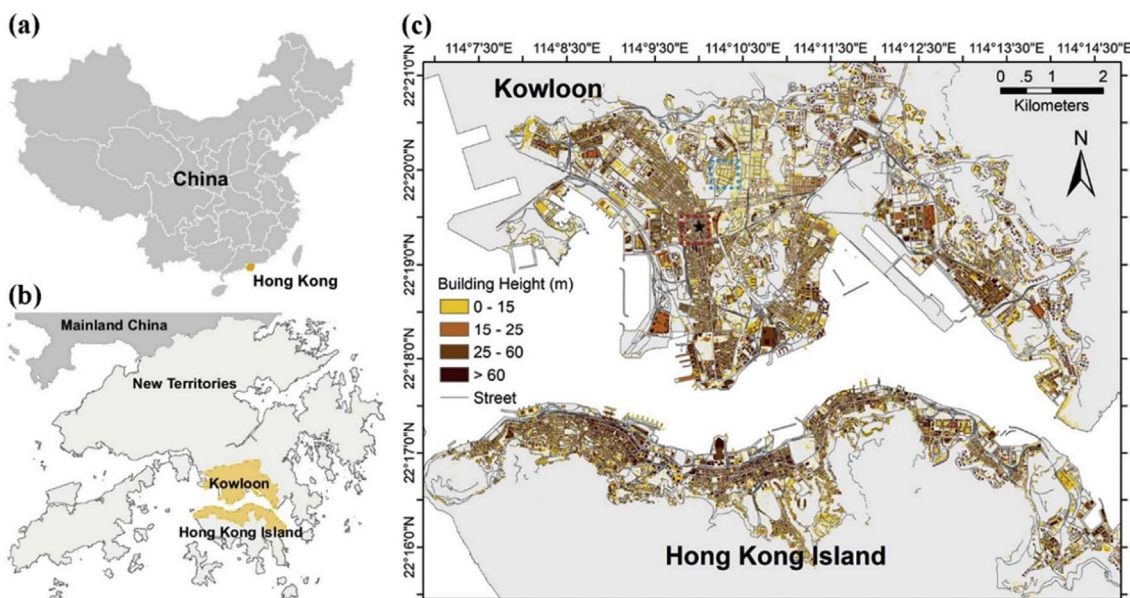


Fig. 2. (a) Location of Hong Kong (yellow circle) in south-eastern China; (b) High-density urban areas in Hong Kong, as outlined in yellow, including Kowloon and northern Hong Kong Island; (c) Building density map, including distribution and height, overlaid with streets in grey. The building and street data are extracted from the B5000 maps series by the Hong Kong Lands Department. The dotted red and blue rectangles outline the field survey regions for high-rise and low-rise regions, respectively, as described in Section 3.3. The black star is the location of the street canyon example in Mong Kok shown in Fig. 1. (For interpretation of the references to color in this figure legend, the reader is referred to the Web version of this article.)

collected using the GSV API [47,48] based on the latitudes and longitudes of the sampling points. Extraction of features, including sky, trees, and buildings, is implemented using the scene parsing method in a deep-learning framework [49,50]. We then project the panorama images from cylindrical to azimuthal projection to generate the fisheye images. From the fisheye images, VFs are calculated by applying the classical photographic method [4]. Fig. 3 shows the workflow procedure for VF calculations using this method, and a detailed description is as follows.

2.2.1. Collecting GSV panorama images

We sampled points at 30 m intervals along the street lines shown in Fig. 2 (c), using GIS software. There is a total of 33,544 sample points in the study area. We collected the GSV panorama images for all the sampled points in the following ways:

- (1) Obtain panorama image ID at a specific location using the following URL:

```
https://maps.googleapis.com/maps/api/streetview/metadata?
size=400x400&location=LAT,LON&heading=HEADING&fov=FOV&
pitch=PITCH&key=APIKey
```

where LAT and LON are the latitude and longitude, respectively, FOV (90 by default) determines the horizontal field of view of the image, HEADING (0 by default) indicates the compass heading of the camera, PITCH (0 by default) specifies the up or down angle of the camera relative to the street view vehicle, and API key is the credential required to authenticate the request.

- (2) Download tiles of a panorama image using the following URL:

```
http://cbk0.google.com/cbk?output=tile&panoid=PANO_ID&
zoom=5&x=I&y=J
```

where PANO\_ID is obtained from the above step; and I (from 0 to 25) and J (from 0 to 12) are the rows and column indices of the image tile. We can get a complete panorama image by combining 26 × 13 tiles. Invalid GSV images, including those with empty content, are

filtered out. Examples of GSV images in high-rise and low-rise areas are shown in Fig. 3 (a).

2.2.2. Extractions of street features using deep-learning techniques

We propose the use of the scene parsing method in a deep-learning framework to extract street features, including sky, trees, and buildings, from the GSV images. The deep-learning model employed in this study is the Pyramid Scene Parsing Network (PSPNet) [49]. In essence, scene parsing segments and parses an image into different image regions associated with semantic categories, including sky, trees, and buildings.

Deep learning based on the deep convolutional neural network (CNN) allows computational models that are composed of multiple processing layers to learn representations of natural data with multiple levels of abstraction and has been widely used in image classification and pattern recognition [51]. Enabled by the proliferation of deep-learning techniques, a number of CNN-based models for semantic scene parsing, such as understanding street features, have been proposed and have achieved outstanding performance [52–54]. Compared with previous work, the architecture of PSPNet pays more attention to feature ensembling and structure prediction, to integrate global context information into the prediction process. The PSPNet model employed in this study provides a fully convolutional network (FCN)-based pixel prediction framework that is superior for processing difficult scenery context features. It is a practical system for state-of-the-art scene parsing and semantic segmentation where all crucial implementation details are included [49]. PSPNet uses a pre-trained semantic segmentation network based on the ADE20K dataset. When evaluating prediction accuracies on various datasets, it achieves state-of-the-art performance and outperforms many other models in the semantic scene parsing framework. In particular, it achieves a high accuracy of 80.2% in predicting 150 object classes of cityscapes, a dataset for semantic urban scene understanding collected from 50 cities in different seasons.

Fig. 4 shows the workflow of semantic scene parsing using PSPNet. The downloaded and combined GSV panorama image is first resampled into 473 × 946 pixels. The panorama image is then separated into two images with 473 × 473 pixels, a size required by the deep-learning module, before consecutively inputting the two images into the PSPNet,

	Example of high-rise area	Example of low-rise area
[Lat, Lon]	[22.3224, 114.1708]	[22.3328, 114.1747]
(a) Panorama image		
(b) Features extraction		
(c) Fisheye image		
[SVF, TVF, BVF]	[0.34, 0.00, 0.65]	[0.64, 0.16, 0.20]

Fig. 3. Workflow procedure for VF calculations using GSV images, illustrated by taking two examples from high-rise and low-rise areas. (a) Panorama images downloaded from Google servers using coordinates of sampling street points as inputs. (b) Extraction of sky (in blue), trees (in green), and buildings (in grey) using the scene parsing deep-learning technique [49]. (c) Fisheye images obtained by projecting the panorama images from cylindrical projection to azimuthal projection. Based on the fisheye image of extracted features, SVF, TVF, and BVF are calculated using the classical photographic method developed by Johnson and Watson [4]. The resulted VF estimates are also indicated. (For interpretation of the references to color in this figure legend, the reader is referred to the Web version of this article.)

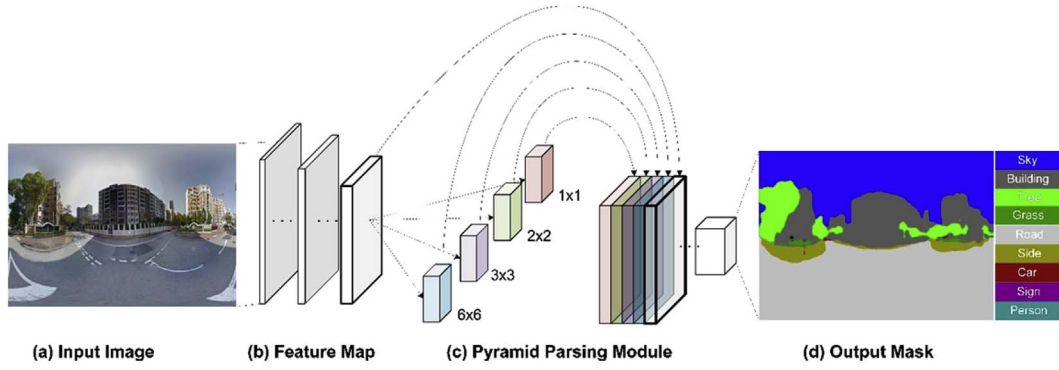


Fig. 4. Workflow of semantic scene parsing using PSPNet. For a given input street view image in (a), the network extracts the feature map in (b), and then the pyramid parsing module is applied to form the final feature representation of the streetscape in (c). Finally, a pixel-wise classified output street view image with semantic categories in (d) is produced by feeding the feature representation into a convolution layer.

as shown in Fig. 4 (a). PSPNet uses CNN to get the feature map of the last convolutional layer as shown in Fig. 4 (b). A pyramid parsing module is applied to harvest different sub-region representations of the image, followed by up-sampling and concatenation layers to form the final feature representation of the streetscape, which carries both local and global context information, as illustrated in Fig. 4 (c). It fuses features under four different pyramid scales with bin sizes of  $1 \times 1$ ,  $2 \times 2$ ,  $3 \times 3$ , and  $6 \times 6$ , respectively. Finally, the representation is fed into a convolution layer to get the final per-pixel prediction and produce a pixel-wise classified street view image with semantic categories in Fig. 4 (d). The size of output images is also  $473 \times 473$  pixels, includes 150 classifications, and features of the sky, trees, and buildings are extracted and calculated in this study. Using a workstation with an eight-core CPU and an NVIDIA 1080Ti GPU (12G RAM), it took about 20 h to finish the 33,544 images, roughly two seconds per panorama image. TVF is general definition vegetation, including grass and trees. Based on the calculation results of 33,544 GSV images using deep learning, values of both SVF and TVF that are zero will be filtered, as these points are distributed indoors or in tunnels after checking the original GSV images. The study uses the filtered 29,264 GSV images for further analysis. Examples of the extracted features are shown in Fig. 3 (b).

### 2.2.3. Projection into fisheye images and calculations of VFs

#### (1) Projection into fisheye images

We use the photographic method, which applies a fisheye lens to the panorama image, in order to project the hemispheric environment (cylindrical projection) onto a circular plane (azimuthal projection) and generate the fisheye image in the following way [34]. This projection is implemented by constructing a relationship between pixels  $(x_f, y_f)$  on a fisheye image and  $(x_p, y_p)$  on a panorama image, given by,

$$x_p = \begin{cases} (\pi/2 + \tan^{-1}[(y_f - C_y)/(x_f - C_x)]) \times W_p/2\pi, & x_f < C_x \\ (3\pi/2 + \tan^{-1}[(y_f - C_y)/(x_f - C_x)]) \times W_p/2\pi, & x_f > C_x \end{cases} \quad (1)$$

$$y_p = \left( \sqrt{(x_f - C_x)^2 + (y_f - C_y)^2} / r_0 \right) \times H_p \quad (2)$$

where  $W_p$  and  $H_p$  are the width and height of the panorama image, respectively;  $r_0 = W_p/2\pi$  is the radius of the fisheye image; and  $(C_x, C_y)$  are the coordinates of the center pixel on the fisheye image;  $C_x = C_y = W_p/2\pi$ . First, an empty fisheye image is initialized with coordinates  $(x_f, y_f)$ . By using equations (1) and (2), each pixel with coordinate of  $(x_f, y_f)$  is then uniquely connected to a pixel with coordinate of  $(x_p, y_p)$  in the panorama image. Lastly, the pixel value in  $(x_f, y_f)$  can be assigned by that in  $(x_p, y_p)$  and this process is repeated for each pixel

until the fisheye image is fully constructed.

#### (2) Calculations of VFs

To calculate VFs with the following Equation (3) based on Johnson and Watson [4], we divide the fisheye image into a number of concentric annuli of equal width, and then sum up all the annular sections representing the sky, trees, and buildings to calculate the SVF, TVF and BVF, respectively, using the following formula:

$$\psi_x = \frac{1}{2\pi} \sin \frac{\pi}{2n} \sum_{i=1}^n \sin \left[ \frac{\pi(2i-1)}{2n} \right] \alpha_{i,x} \quad (3)$$

where  $x$  can be sky, tree, or building;  $n$  is the total number of rings (here we use 100);  $i$  (from 1 to 100) is the index of the ring;  $\alpha_{i,x}$  is the angular width of pixels of feature  $x$  ( $x$  can be sky, tree, or building) in the  $i$ th ring. Examples of the generated fisheye images are shown in Fig. 3 (c). The SVF, TVF, and BVF quantify the fractions of sky, trees, and buildings, respectively, of the built environment seen from a particular observation point on the ground within the built environment.

#### 2.2.4. Accuracy assessment of feature extraction from GSV images by deep-learning technique

To assess the accuracy of the scene parsing deep-learning technique in extracting street scenes, especially for the VFs of the sky, trees, and buildings, the focus of this study, we randomly select 100 sampled street points and collect their corresponding GSV images. The 100 selected samples are randomly distributed in the study area and cover low-to-high building densities (see Fig. A.1), indicating these samples represent different characteristics of street canyons and street trees. Manual delineation of the images by eye inspection is implemented to extract the sky feature to generate a reference dataset (as truth). As a result, Fig. 5 shows the comparison of calculated VFs from GSV images based on the deep-learning technique and the generated reference data. The two datasets nearly exactly agree with each other, with  $R^2$  as high as 0.974 and RMSE of 0.036 for SVF,  $R^2$  of 0.986 and RMSE of 0.025 for TVF, and  $R^2$  of 0.983 and RMSE of 0.037 for BVF. This agreement suggests that the scene parsing deep-learning technique is able to accurately extract the street-level features in high-density urban areas of Hong Kong.

### 2.3. 3D-GIS-based SVF estimates

The high-resolution 3D-GIS-based SVF estimate of Hong Kong was developed by Chen et al. (2012) [32] to study Hong Kong's urban microclimate. The 3D-GIS Model is generated in a geographic information system (GIS) by using a 3D building database (with building height information) merged with the topography database to create a digital elevation layer representing the height of the urban surface in Hong

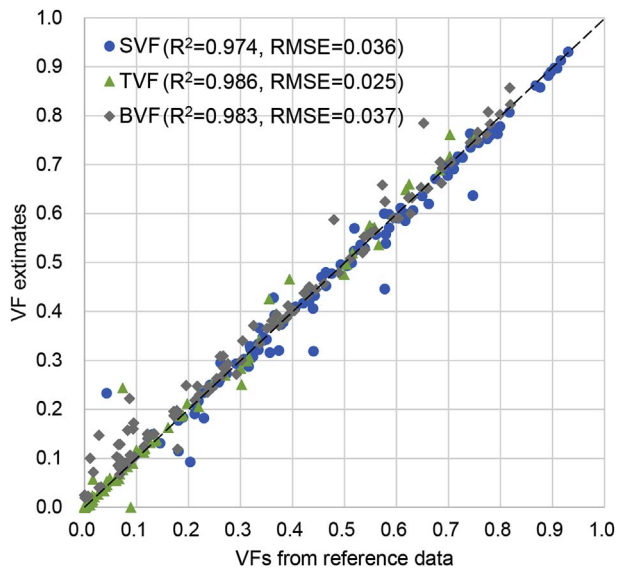


Fig. 5. Accuracy assessment of feature extraction using the PSPNet in a deep-learning framework to calculate SVF, TVF, and BVF from GSV images in high-density urban areas of Hong Kong. The  $R^2$  and RMSE between the two datasets of VFs are also indicated.

Kong. Both 3D building and topography databases are provided by the Hong Kong Planning Department. Continuous SVF values at 2 m resolution are calculated for an entire urban environment. The SVF is calculated by first constructing a fisheye image and then estimating the SVF value using Equation (3) based on Johnson and Watson [4], the same method used with GSV images as described in Section 2.2.

In this study, SVF estimates from the 3D-GIS model are compared with those from GSV, as described in Section 3.3, for the purpose of assessing the accuracy of urban 3D-GIS model in simulating urban street environments under high-density contexts. This comparison is important because: (1) 3D-GIS models have been widely used to estimate the street geometric structures, including SVF, but a comprehensive verification in a wide region is not possible because conventional

verification methods are both time and effort consuming [32]; (2) the GSV-based method makes it possible to map the SVF at street level across the whole city, and therefore, as this study shows, a comprehensive verification of the 3D-GIS model can be conducted. The understanding of the discrepancies between GSV-based and 3D-GIS-based SVF estimates sheds light on future improvement in the model simulation of complex urban environments.

### 3. Results

#### 3.1. Mapping SVF, TVF, and BVF of street canyons using GSV images

Fig. 6 shows the spatial distributions of GSV-based SVF, TVF, and BVF estimates in high-density urban areas in Kowloon and Hong Kong Island, and a comparison of their frequency distributions. The mean SVF, TVF, and BVF values in high-density areas of Hong Kong are 0.49, 0.14, and 0.33, respectively, and there are small differences between Kowloon area (0.53, 0.12, and 0.41) and Hong Kong Island (0.41, 0.19, and 0.36). The SVF value ranges from near 0, indicating little sky openness, to 1.0, indicating total sky openness. In general, we found the spatial patterns of VF estimates are similar and consistent with the corresponding building height and density (see Fig. 2 (c)). Areas with higher density have lower SVF, lower TVF and higher BVF, and vice versa. The high-density residential areas, located in southern and western Kowloon and northern Hong Kong Island, which cover about 58% of the study area, are dominated by low and moderate SVF (0.2–0.6), and low TVF (0.0–0.3), because of the high-density construction and narrow streets that block sky visibility and limit space for greenery. The coastline regions and low-rise areas, which cover about 20% of the study area, show much higher SVF (0.7–1.0), and lower BVF (0.0–0.3), because of fewer buildings and more sky openness.

In low-rise regions near country parks in the southern part of the study area in Hong Kong Island where BVF is low (e.g., the dotted rectangles in Fig. 6), the SVF values, however, are in a much lower range (0.0–0.2; Fig. 6 (c)). The much lower sky openness, as we discuss later, is mainly due to high tree cover in this area (Fig. 6 (b)), which blocks much of the sky visibility. Further analysis of the impact of tree cover is described in Section 3.4. Fig. 6 (d) shows the frequency

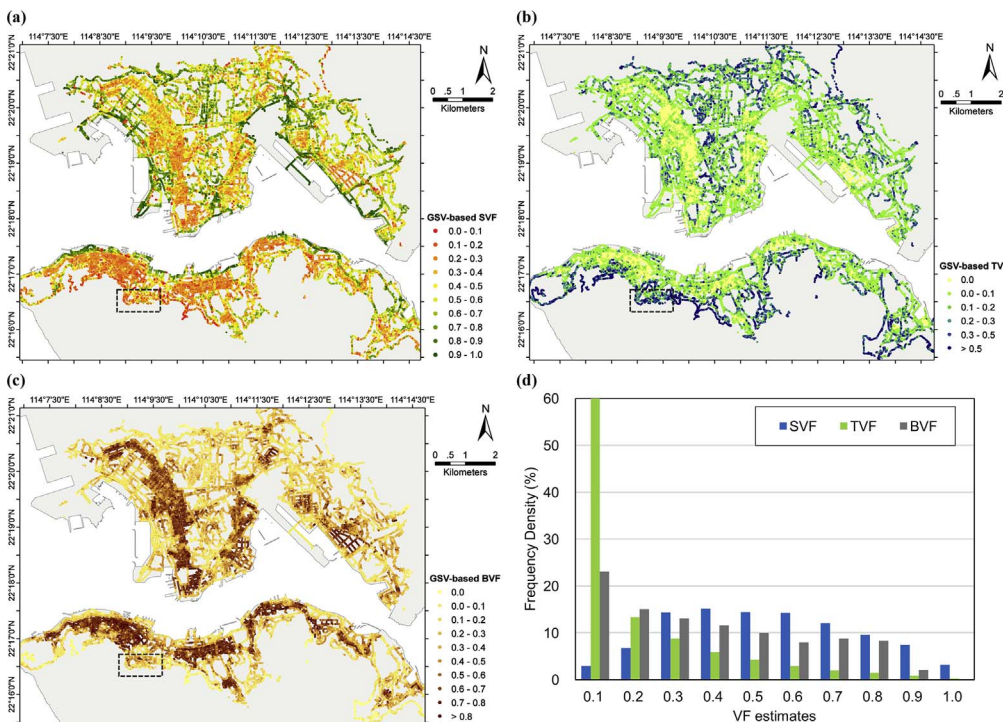


Fig. 6. Maps of GSV-based SVF in (a), TVF in (b), and BVF in (c) of street canyons in high-density urban areas of Hong Kong derived from 29,264 GSV images along streets at 30 m intervals; (d) Frequency density of SVF (blue bar), TVF (green bar), and BVF (grey bar). (For interpretation of the references to color in this figure legend, the reader is referred to the Web version of this article.)

distribution of the VFs in Hong Kong. The TVF in the high building density area is dominated by values less than 0.1 and the mean value is 0.143. The low TVF is mainly limited by the high building density and narrow streets. This mean TVF is smaller compared with Singapore (0.293), a sub-tropical Asian city with high building and population densities, and is similar to New York (0.135), a typical high-density city in the United States [55]. SVF, on the other hand, is close to an even distribution between 0.2 and 0.9, with a peak between 0.4 and 0.5, while BVF has a decreasing frequency when its value increases.

### 3.2. Verification of GSV-based VF estimates

The comparison of VF estimates and direct measurements using hemispherical photography is a convincing way to verify the effectiveness and assess the uncertainties associated with GSV-based and 3D-GIS-based methods for estimating VFs of street canyons. Here we use fisheye lens hemispheric photography to verify the applicability of GSV-based and 3D-GIS-based methods in high-density urban areas of Hong Kong. This is, to our knowledge, the first reported use of hemispheric photography for direct verification of a GSV-based streetscape study.

Forty photographs were taken at 40 selected sample points (20 in the high-rise area of Mong Kok and 20 in the low-rise area of Kowloon Tong) in Kowloon, as shown in Fig. 2 (c). The photographs were taken at 1.5 m above ground level, using a digital camera, Nikon FM601, with an 8-mm circular lens. Fig. 7 shows four examples of photographs taken with a fisheye lens in our field survey (a) and the collocated projected GSV fisheye images (b). The feature extraction results and the corresponding VF estimates are also shown. The field survey results are consistent with GSV-based estimates, with differences within 0.03, suggesting the effectiveness and high accuracy of using GSV images in estimating VFs in high-density urban areas of Hong Kong.

Fig. 8 illustrates the comparisons of survey-based reference VF data and GSV-based and 3D-GIS-based VF estimates. The GSV-based method we propose to use in high-density urban areas of Hong Kong performs much better in estimating SVF (Fig. 8 (a)) than the commonly used 3D-GIS-based method, with higher  $R^2$  (0.954 versus 0.014) and lower RMSE (0.033 versus 0.263). In particular, 3D-GIS has higher  $R^2$  in high-

rise areas than in low-rise building areas, indicating that model simulation performs better in high-rise building areas. Moreover, for GSV-based estimates,  $R^2$  and RMSE for TVF (Fig. 8 (b)) are 0.987 and 0.027, respectively, and for BVF (Fig. 8 (c)) they are 0.986 and 0.036, respectively. These results suggest that a GSV-based streetscape study is effective and accurate in high-density urban areas of Hong Kong, characterized by compact high-rise areas with complicated street environments and by low-rise areas with dense tree canopy.

### 3.3. Comparison between GSV-based and 3D-GIS-based SVF estimates

In this section, the collocated SVF estimates at 30 m intervals derived from GSV and 3D-GIS Model are compared for the purpose of assessing the accuracy of urban 3D-GIS model in simulating the urban street environment in high-density contexts. Fig. 9 (a) illustrates the spatial distribution of 3D-GIS-based SVF estimates at 30 m intervals in high-density areas of Hong Kong, corresponding to the sampling points in Fig. 6 (a). The map of 3D-GIS-based SVF shows a similar pattern to that of GSV-based SVF estimates, in which the lower SVF values are located mainly in areas with high-rise buildings and higher SVF values located in low-rise or coastal areas. The mean SVF value of 3D-GIS-based estimates (0.59) is about 0.11 (about 20%) higher than that of GSV-based estimates (0.49) but with the similar standard deviation (0.234 and 0.225, respectively). However, there are large differences in the low-rise areas with large quantities of street trees. To investigate the spatial difference, Fig. 9 (b) shows the spatial distribution of the difference between 3D-GIS-based and GSV-based SVF estimates (former minus latter). The two datasets have a better agreement in high-rise regions (difference less than 0.1) than the regions with lower building rise (difference larger than 0.1). This characteristic of difference can also be seen from the bivariate histogram in Fig. 9 (c), which shows that (1) GSV-based and 3D-GIS-based SVF estimates have good agreement (the highest data number density can be seen in the diagonal direction) in high-rise regions with small SVF between 0.2 and 0.4. Out of all the sampling points, 43.85% of them have a difference larger than 0.1; (2) some 3D-GIS-based values are higher than GSV-based values, suggesting model simulations overestimate the SVF in some regions.

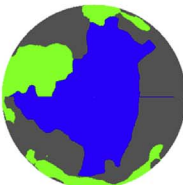
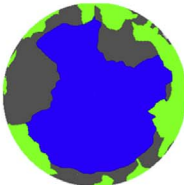
	High-rise areas		Low-rise areas	
[Lat, Lon]	[22.3224, 114.1708]	[22.3245, 114.1700]	[22.3328, 114.1747]	[22.3341, 114.1755]
(a) Field Survey				
[SVF, TVF, BVF]	[0.32,0.00,0.67]	[0.32,0.03,0.65]	[0.62, 0.19,0.19]	[0.74,0.13,0.13]
(b) GSV-based				
(c) Feature Extraction				
[SVF, TVF, BVF]	[0.34, 0.00, 0.65]	[0.33, 0.01, 0.66]	[0.64, 0.16, 0.20]	[0.77, 0.12, 0.11]

Fig. 7. Examples of fisheye images from two high-rise and two low-rise street sample points from field surveys in (a), and GSV-based method in (b). Image features are classified into the sky (in blue), trees (in green), and buildings (in grey) using the scene parsing deep-learning technique, as shown in (c). SVF, TVF, and BVF values from field surveys and GSV are shown as indicated. (For interpretation of the references to color in this figure legend, the reader is referred to the Web version of this article.)

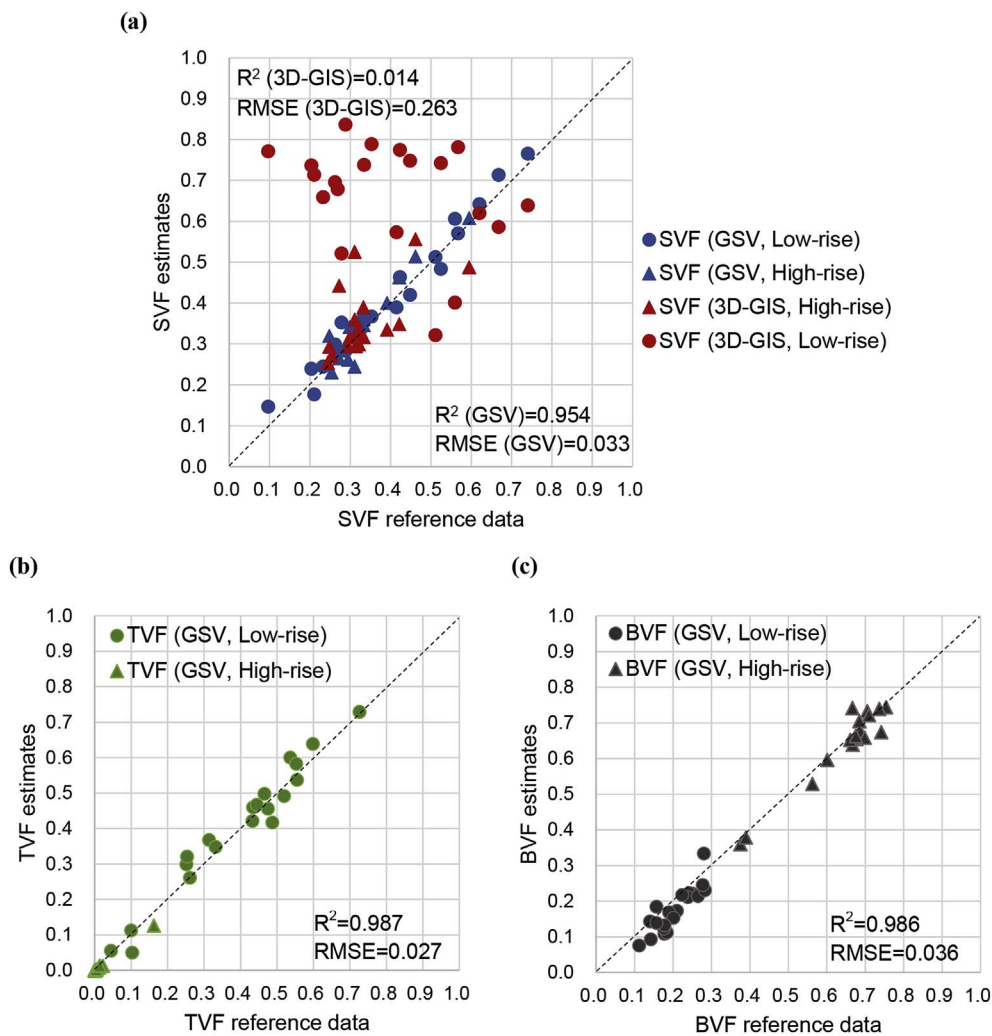


Fig. 8. (a) Scatter plot of SVF reference data from field survey and the corresponding GSV-based (in blue) and 3D-GIS-based (in red) SVF estimates. Sampling SVF data include 20 samples in Mong Kok within high-rise building area (in triangles), and 20 samples in Kowloon Tong within low-rise building area (in circles); (b) the same as (a) but for TVF; (c) the same as (a) but for BVF. (For interpretation of the references to color in this figure legend, the reader is referred to the Web version of this article.)

According to the descriptive statistics of the 29,264 sample points from this comparison, the  $R^2$  between them is 0.40 with RMSE of 0.22. This overestimation of SVF by the 3D-GIS-based method can also be seen in the histogram plots in Fig. 9 (d), which shows that the 3D-GIS-based method has shifted the peak of the frequency distribution of SVF from less than 0.5 to larger than 0.5. As a result, the mean SVFs are different by 0.11. The contributors to this pattern of difference are investigated in Section 3.4.

### 3.4. Impacts of street tree canopy and building density on SVF estimates

To gain further understanding of the discrepancies between GSV-based and 3D-GIS-based SVF estimates and shed light on future improvements in the model simulation of the urban environment, we investigate the impacts of the street tree canopy, quantified using the TVF estimate, and building density, quantified using the BVF estimate, on the discrepancies shown in Fig. 9.

The bivariate histogram of GSV-based TVF and the difference between GSV-based and 3D-GIS-based SVF estimates is presented in Fig. 10 (a). We can see that (1) a large majority of the data has small differences (close to 0) and low TVF (smaller than 0.2) and (2) there is a strong positive correlation between TVF and the difference. When TVF is larger than 0.1,  $R^2$  of the two datasets is 0.53 ( $p < 0.01$ ), indicating a significant correlation. This result indicates that a higher number of

street trees leads to a larger difference between estimations of SVF from GSV images and 3D-GIS simulation, especially when the TVF is larger than 0.1. The result from linear regression shows that the increase of the difference follows the increase of TVF by a factor of 1.17. This strong correlation suggests that TVF, an indicator of the number of street trees, makes the dominant contribution to the discrepancies between GSV-based and 3D-GIS-based SVF estimates. This is because model simulations cannot parameterize street trees well due to their complexity, leading to underrepresentation of model simulations of realistic street environments. Therefore, in general, the 3D-GIS-based method produces larger sky openness and overestimate the SVF of street canyons in high-density urban areas in Hong Kong. This result differs from the study [35] in the less dense Cardiff, UK, which indicates no significant correction between the difference in SVF estimates and street trees.

Fig. 10 (b) illustrates the bivariate histogram of GSV-based BVF, an indicator of building density, and the difference between the two SVF estimates. We can see that (1) most data differ between  $-0.1$  and  $0.1$  and correspond to a wide range of BVFs from 0 to 0.9, and (2) when BVF is large, that is when building density is relatively large, the difference is centered at 0 with a small variation range, indicating good performances of model simulations in high-rise areas of Hong Kong. On the other hand, when BVF is small, the difference tends to be positive, indicating that the 3D-GIS-based SVF estimate is higher than the GSV-

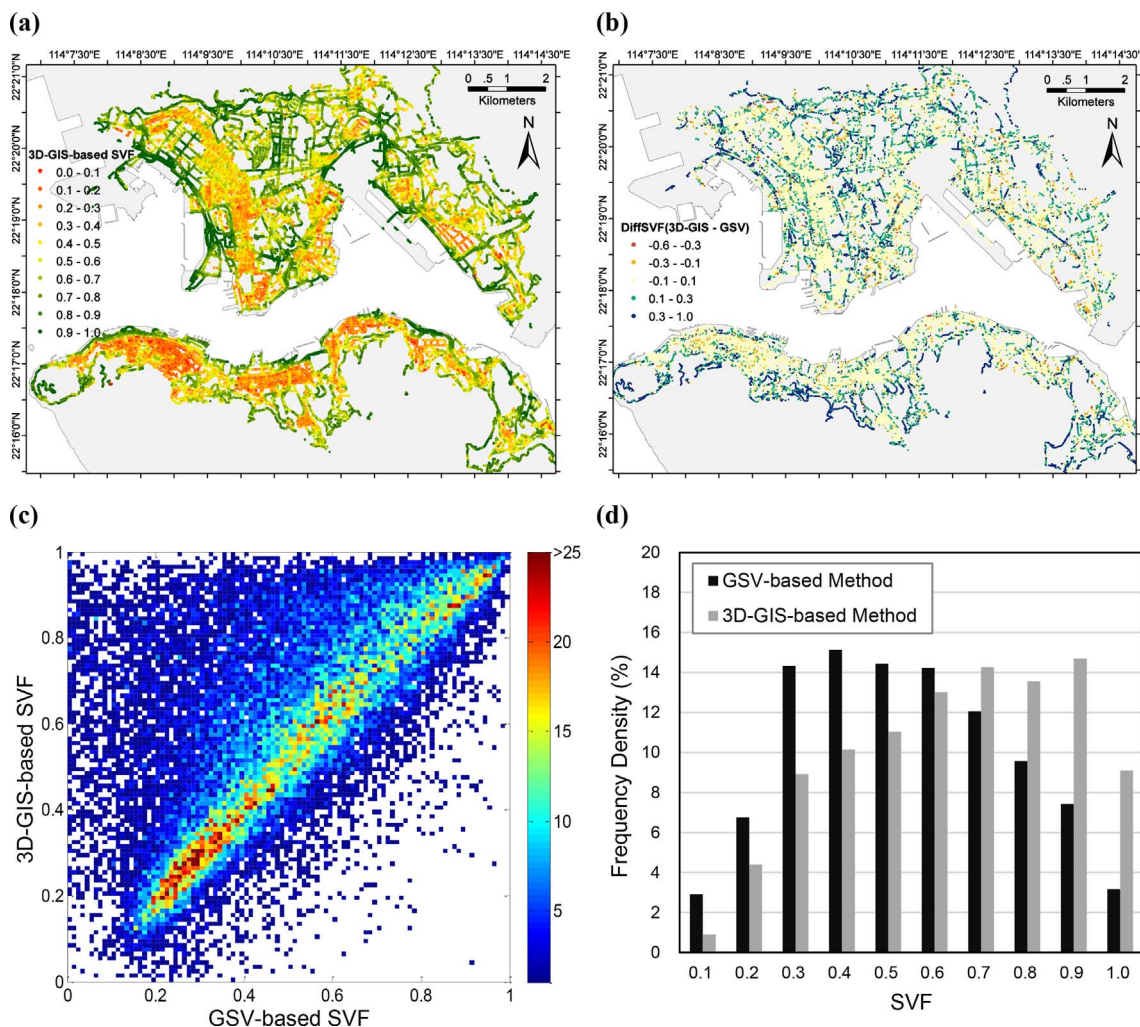


**Fig. 9.** (a) Map of 3D-GIS-based SVF estimate with the same street sampling points as Fig. 6 (a); (b) Map of the difference between GSV-based and 3D-GIS-based SVF estimates; (c) Bivariate histogram of GSV-based and 3D-GIS-based SVF estimates of street canyon in high-density urban areas of Hong Kong as shown in Figs. 6 (a) and 9 (a), respectively. To make the histogram, the SVF data from both datasets are grouped into  $0.01 \times 0.01$  grids and the value of a grid is the total number of SVF samples that fall in this grid; (d) Comparison of frequency density histogram from GSV-based and 3D-GIS-based SVF estimates.

based estimate in lower density regions. Especially when BVF is close to 0, that is in the urban areas with very low building density, the differences can be very large, probably mainly due to the impact of trees, as shown in Fig. 10 (a). This figure shows that the lower the building density, the greater the difference. Combined with the effect of street trees on SVF values in Fig. 10 (a), our study shows that the larger amounts of street trees are associated with a higher uncertainty of modeled SVF. On the other hand, the higher the building density, the smaller the uncertainty.

#### 4. Discussion

##### 4.1. High-accuracy VF estimates for better modeling of urban thermal environment

The climate of Hong Kong during hot and humid summer causes thermal discomfort and decreases the quality of living, and both effects are intensified by the UHI effect in heavily built-up areas. Serious issues related to human thermal comfort [56], air pollution [57,58] and the UHI effect [59,60] due to its climate and urban morphologies have been primary planning concerns in Hong Kong. The urban radiation balance and thermal environment are crucially affected by the geometry and structures of street canyons [61]. There is a pressing need for high-accuracy estimates of SVF, TVF, and BVF, which are effective indicators

of the geometry and structures of street canyons.

This study proposes the use of publicly available GSV panorama images and a deep-learning technique to estimate the SVF, TVF, and BVF of street canyons in high-density urban areas of Hong Kong. From the verification results against reference data (as truth), the GSV-based VFs show a satisfying agreement (with all  $R^2$  values larger than 0.95) with the reference data. This result indicates the high accuracy of estimating VFs using GSV images and the deep-learning technique. These high-accuracy estimates will improve the calculation of urban thermal radiation in modeling the street canyon thermal environment in Hong Kong. Moreover, the GSV-based method developed is capable of providing more detailed VF estimates at various scales from a small site to an entire city. Since GSV images are available in many cities all over the world, this method provides a low-cost and effective approach to support global studies of urban thermal environments.

##### 4.2. Large uncertainty in model-based SVF estimates from street trees

With the availability of 3D-GIS models for urban areas, the SVF can be continuously estimated at large spatial scales by simulating and calculating the projection of building blocks from any point on the ground. However, due to its complexity in shape and structure, street tree canopy information, a major feature of urban settings, is usually very difficult to parameterize and incorporate in models. As our study

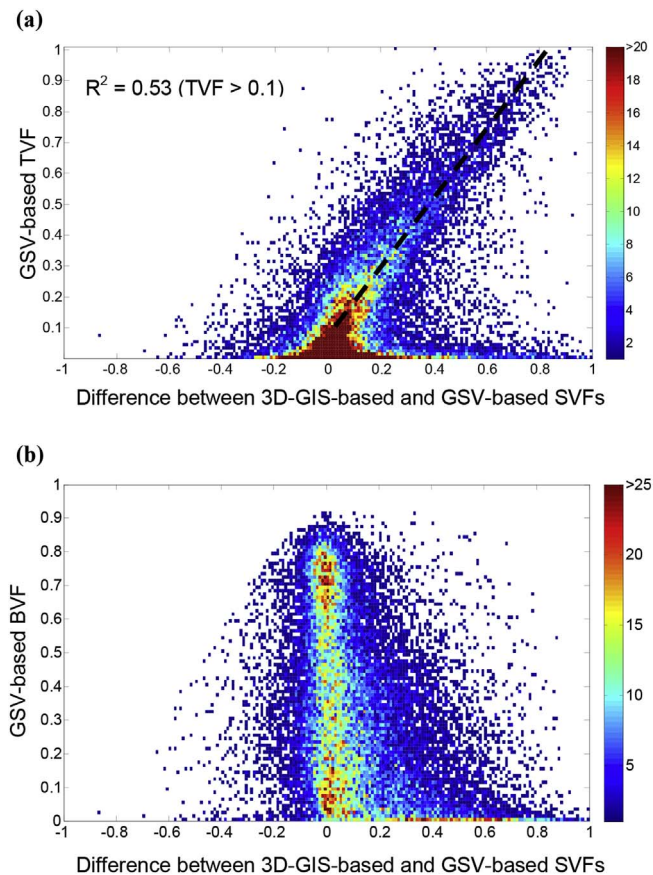


**Fig. 10.** (a) Bivariate histogram of GSV-based TVF and the difference between 3D-GIS-based and GSV-based SVFs (former minus latter). As indicated, when TVF > 0.1, the  $R^2$  is 0.53 and the best fit linear slope is 1.17 (in dotted black line); (b) Bivariate histogram of GSV-based BVF and the difference between 3D-GIS-based and GSV-based SVFs (former minus latter). To derive the histogram, the data from both datasets are grouped into  $0.01 \times 0.01$  grids and the value for each grid is the total number of SVF samples that fall in the grid.

shows, the 3D-GIS-based method captures well the spatial pattern and variability of SVF in high-density urban areas of Hong Kong. However, it overestimates SVF by 0.11 on average. Moreover, our results show that as TVF increases by one unit, the resulting SVF error from the 3D-GIS-based method decreases by 1.17 unit, suggesting a significant correlation ( $R^2 = 0.53$ ;  $p < 0.01$ ) between street trees and the errors in model simulations. This result suggests that a lack of street trees is the dominant factor contributing to the large uncertainties in model simulations of urban street geometry. On the other hand, based on the linkage between street trees and the difference between 3D-GIS-based and GSV-based SVF estimates, the shade provision of street trees in urban street canyons can be estimated using GSV images [34]. Street-level imagery allowed us to consider obstructions along street canyons without relying on simplifications or simulations of the environment.

#### 4.3. Temporal variation of street-level VFs

Hong Kong is located in a subtropical monsoon region with little effect of seasonality on the variation of the street tree canopy. A specific assumption on the seasonality is that the leaf cover of street trees does not change during different seasons even though the acquisition time of GSV images differs (see Fig. A.2). This is a reasonable assumption since Hong Kong is located in the subtropical monsoon region where the street trees can be maintained throughout the year [62]. Moreover, Hong Kong is a highly developed high-density city where the built-up areas are limited and therefore very little change has taken place during recent years [40] that will significantly affect the street skylines.

However, for temperate climate regions, the seasonality of TVF will be a big issue, given that the street trees will be in an annual cycle of greening during growing seasons, and turning yellow and falling during the autumn and winter seasons. The change in color of tree leaves poses a challenge for VF studies using conventional tree detection method based on the traditional spectral (RGB) information. The developed deep-learning method in this study, on the other hand, extracts street features based on local and global context information independent of spectral information. Therefore, it has an advantage over the traditional pixel-based spectral method. The developed method in this study can be used to address the problem of VF seasonality by first training the deep-learning module with tree image samples from different seasons and then applying it to GSV images grouped into different seasons (see Fig. A.2(b)).

#### 4.4. Limitations and future studies

The GSV-based method is applicable only in areas with GSV images for mapping streetscape variables, including SVF, BVF, and TVF. In areas without GSV data, such as the areas on Hong Kong Island, the 3D-GIS-based method or DSM-based method is still effective. The conclusions from studying the impact of street trees and building density on the uncertainty of the 3D-GIS-based method contribute to the future improvement of modeling the urban street environment. In this study, we use a 30 m interval for calculating VFs, assuming that this resolution would suffice to resolve the variation of VFs within a street. However, the GSV-based method is flexible in using any interval for mapping VFs of street canyons for study areas with different spatial scales.

GSV images may have the potential to investigate the symmetric and asymmetric characters of street canyons [63,64] with the following extra inputs and assumption, including the exact location of the observer, the width of the street which enables accurately calculating the observer position relative to both sides of the street, and assuming street trees don't block buildings on both sides. In this way, the height of buildings on both site along the street can be calculated and the asymmetric characters of street canyons may be determined.

In addition, sun view factor which is relevant to daytime shortwave irradiance can also be estimated by constructing geometries and orientations of street canyons using GSV images [36]. The estimation involves the projection of the sun trajectory on the GSV fisheye image and then the calculation of the fraction of the length of solar trajectory within the sky view range when sunlight can be seen. The quantification of street sun view factor compares the number of points of a sun path not blocked by obstacles with the total amount of points in the sun path in GSV images. It is critical for quantifying the sun-exposure of the solid surfaces, which is needed to resolve the heterogeneity in urban areas for estimating thermal comfort more accurately.

## 5. Conclusions

This study focuses on (1) developing an approach for accurately deriving VFs for the sky, trees, and buildings of street canyons in the high-density urban environment of Hong Kong using publicly available GSV images and a deep-learning feature extraction algorithm; (2) verifying the accuracy of the developed GSV-based method using reference data of hemispheric photography from field surveys; and (3) comparing the GSV-based and 3D-GIS-based VF estimates and investigating the impact factors for the discrepancies between them. As a result, maps of SVF, TVF, and BVF of street canyons in high-density urban areas of Hong Kong are generated. The mean SVF, TVF, and BVF values in high-density areas of Hong Kong are 0.49, 0.14, and 0.33, respectively. The following conclusions can be drawn:

- The spatial patterns of VF estimates are similar and consistent with the corresponding building height and density. The TVF is dominated by values less than 0.1, which is limited by the high building

density and narrow street environment.

- Verification using reference data by hemispheric photography from field surveys shows that the GSV-based VF estimates have a satisfying agreement (with all  $R^2$  values larger than 0.95) with the reference data. It suggests the effectiveness and high accuracy of the GSV-based method.
- A comparison between GSV-based and 3D-GIS-based SVFs show that the two SVF estimates are correlated (with  $R^2$  of 0.40) and have a better agreement in high-building-density areas. However, the 3D-GIS-based method overestimates SVF by 0.11 on average.
- The differences between the two methods are significantly correlated with street trees ( $R^2 = 0.53$ ). The more street trees, the larger the difference (by a factor of 1.17). This suggests that a lack of street trees in a 3D-GIS model of a street environment is the dominant factor contributing to the large discrepancies between the two datasets. This study demonstrates an effective and accurate approach for mapping SVF in high-density areas of Hong Kong and suggests

that street trees should be considered in model simulations of urban street environments.

The developed method for analyzing VFs in a 3D street environment will play an important role in relating science-based evidence for urban climatic studies and decision-making in urban planning and design processes.

### Acknowledgment

The study is supported by the Postgraduate Scholarship (PGS) and the Global Scholarship Programme for Research Excellence from The Chinese University of Hong Kong. The authors also wish to give special thanks to the three reviewers for their valuable comments and suggestions that help to improve our research. We also thank the editors for their patient and meticulous work for our manuscript.

## Appendix A

### A.1. Spatial distribution of the 100 random samples

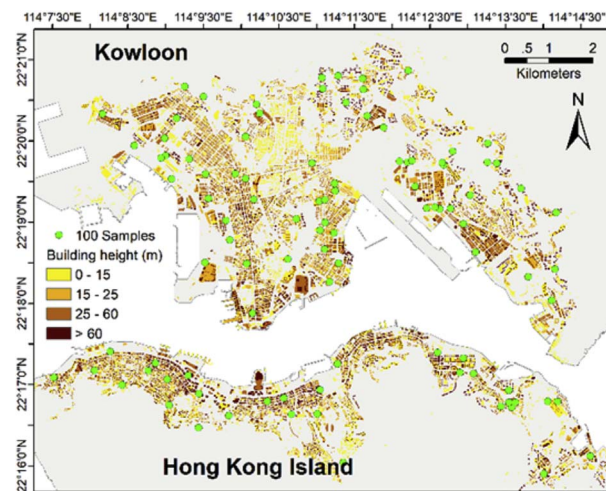


Fig. A.1. Spatial distribution of the 100 randomly selected samples in the study area for verification described in Section 2.2.4. The sampling is implemented by generating 100 random integers using a pseudorandom integer generator in MATLAB to extract data from the total 29,264 street data points.

### A.2. Acquisition time of GSV images

Fig. A.2 shows the spatial distribution of the acquisition time of all the 22,729 GSV images collected in the high-density urban area of Hong Kong, including year in (a) and season in (b). The time information can be extracted from the GSV metafile as described in Section 2.2.1 and shows that 77.7% of the GSV images used in this study were updated and collected during the winter season from December 2016 to January 2017. Some GSV images haven't been updated, which may be due to uncontrolled factors (weather, road closures, etc.) that prevent Google cars from operating [65].

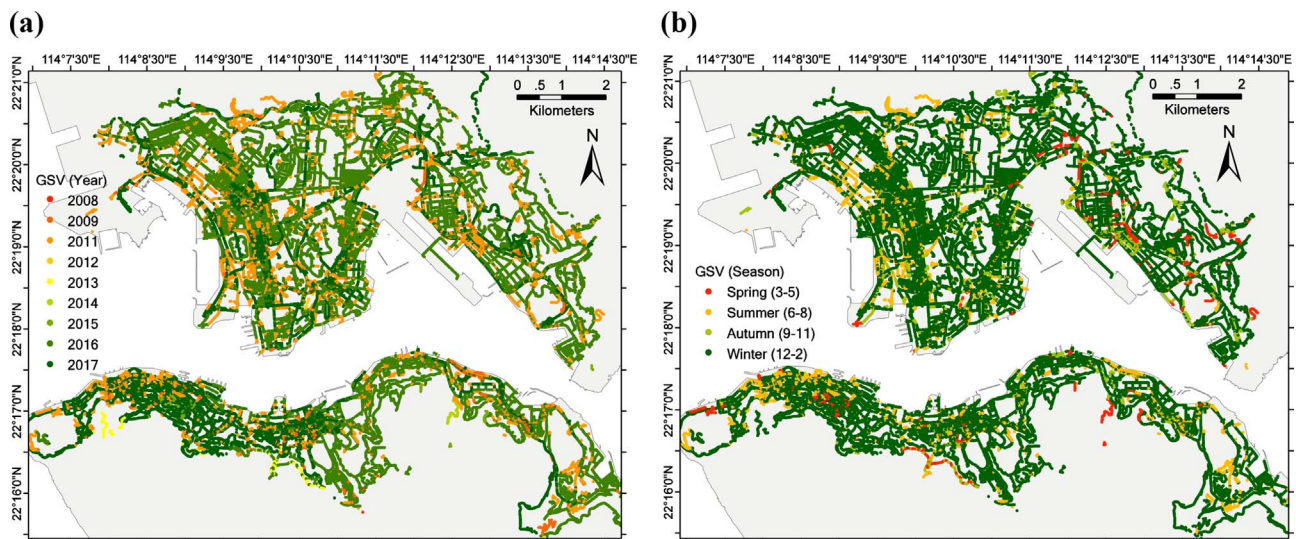


Fig. A.2. Spatial distribution of the acquisition time, including year in (a) and season in (b), of the GSV images this study collected in the high-density urban area of Hong Kong.

## References

- G.S. Brager, R.J. de Dear, Thermal adaptation in the built environment: a literature review, *Energy Build.* 27 (1) (Feb. 1998) 83–96.
- I. Saito, O. Ishihara, T. Katayama, Study of the effect of green areas on the thermal environment in an urban area, *Energy Build.* 15 (3) (Jan. 1990) 493–498.
- E. Johansson, R. Emmanuel, The influence of urban design on outdoor thermal comfort in the hot, humid city of Colombo, Sri Lanka, *Int. J. Biometeorol.* 51 (2) (Nov. 2006) 119–133.
- G.T. Johnson, I.D. Watson, The determination of view-factors in urban canyons, *J. Clim. Appl. Meteorol.* 23 (2) (Feb. 1984) 329–335.
- T.R. Oke, *Boundary Layer Climates*, Routledge, 1987.
- I.D. Watson, G.T. Johnson, Graphical estimation of sky view-factors in urban environments, *J. Climatol.* 7 (2) (Mar. 1987) 193–197.
- E. Johansson, Influence of urban geometry on outdoor thermal comfort in a hot dry climate: a study in Fez, Morocco, *Build. Environ.* 41 (10) (Oct. 2006) 1326–1338.
- F. Bourbia, F. Boucheriba, Impact of street design on urban microclimate for semi arid climate (Constantine), *Renew. Energy* 35 (2) (Feb. 2010) 343–347.
- T.R. Oke, Canyon geometry and the nocturnal urban heat island: comparison of scale model and field observations, *J. Climatol.* 1 (3) (Jul. 1981) 237–254.
- J. Unger, Intra-urban relationship between surface geometry and urban heat island: review and new approach, *Clim. Res.* 27 (3) (2004) 253–264.
- E.L. Krüger, F.O. Minella, F. Rasia, Impact of urban geometry on outdoor thermal comfort and air quality from field measurements in Curitiba, Brazil, *Build. Environ.* 46 (3) (Mar. 2011) 621–634.
- U.W. Tang, Z.S. Wang, Influences of urban forms on traffic-induced noise and air pollution: results from a modelling system, *Environ. Model. Software* 22 (12) (Dec. 2007) 1750–1764.
- X.-X. Li, L.K. Norford, Evaluation of cool roof and vegetations in mitigating urban heat island in a tropical city, Singapore, *Urban Clim.* 16 (Supplement C) (Jun. 2016) 59–74.
- E. Ng, L. Chen, Y. Wang, C. Yuan, A study on the cooling effects of greening in a high-density city: an experience from Hong Kong, *Build. Environ.* 47 (Supplement C) (Jan. 2012) 256–271.
- S. Oliveira, H. Andrade, T. Vaz, The cooling effect of green spaces as a contribution to the mitigation of urban heat: a case study in Lisbon, *Build. Environ.* 46 (11) (Nov. 2011) 2186–2194.
- L. Shashua-Bar, I.X. Tsiros, M.E. Hoffman, A modeling study for evaluating passive cooling scenarios in urban streets with trees. Case study: Athens, Greece, *Build. Environ.* 45 (12) (Dec. 2010) 2798–2807.
- R.A. Sutherland, J.F. Bartholic, Significance of vegetation in interpreting thermal radiation from a terrestrial surface, *J. Appl. Meteorol.* 16 (8) (Aug. 1977) 759–763.
- A.V. Parisi, M.G. Kimlin, J.C.F. Wong, M. Wilson, Diffuse component of solar ultraviolet radiation in tree shade, *J. Photochem. Photobiol. B* 54 (2) (Feb. 2000) 116–120.
- L. Shashua-Bar, M.E. Hoffman, The Green CTTC model for predicting the air temperature in small urban wooded sites, *Build. Environ.* 37 (12) (Dec. 2002) 1279–1288.
- K.V. Abhijith, S. Gokhale, Passive control potentials of trees and on-street parked cars in reduction of air pollution exposure in urban street canyons, *Environ. Pollut.* 204 (Supplement C) (Sep. 2015) 99–108.
- W. Klemm, B.G. Heusinkveld, S. Lenzholzer, B. van Hove, Street greenery and its physical and psychological impact on thermal comfort, *Landsc. Urban Plann.* 138 (Supplement C) (Jun. 2015) 87–98.
- D.R. Richards, P.J. Edwards, Quantifying street tree regulating ecosystem services using Google Street View, *Ecol. Indic.* 77 (Supplement C) (Jun. 2017) 31–40.
- H.J. Fernando, *Handbook of Environmental Fluid Dynamics, Volume Two: Systems, Pollution, Modeling, and Measurements* vol. 2, CRC press, 2012.
- M. Roth, W.T.L. Chow, A historical review and assessment of urban heat island research in Singapore, Singapore, *J. Trop. Geogr.* 33 (3) (Nov. 2012) 381–397.
- Wong Nyuk Hien and Jusuf Steve Kardinal, Air temperature distribution and the influence of sky view factor in a Green Singapore estate, *J. Urban Plann. Dev.* 136 (3) (Sep. 2010) 261–272.
- T.R. Oke, The micrometeorology of the urban forest, *Phil. Trans. Roy. Soc. Lond. B* 324 (1223) (Aug. 1989) 335–349.
- A. Henderson-Sellers, *Future Climates of the World*, Elsevier, 1995.
- M.C. Anderson, Studies of the woodland light climate: I. The photographic computation of light conditions, *J. Ecol.* 52 (1) (1964) 27–41.
- D.G. Steyn, The calculation of view factors from fisheye-lens photographs: research note, *Atmos.-Ocean* 18 (3) (Sep. 1980) 254–258.
- C. Ratti, P. Richens, Raster analysis of urban form, *Environ. Plann. Des.* 31 (2) (Apr. 2004) 297–309.
- T. Gál, F. Lindberg, J. Unger, Computing continuous sky view factors using 3D urban raster and vector databases: comparison and application to urban climate, *Theor. Appl. Climatol.* 95 (1–2) (Jan. 2009) 111–123.
- L. Chen, et al., Sky view factor analysis of street canyons and its implications for daytime intra-urban air temperature differentials in high-rise, high-density urban areas of Hong Kong: a GIS-based simulation approach, *Int. J. Climatol.* 32 (1) (Jan. 2012) 121–136.
- J. Liang, J. Gong, J. Sun, J. Liu, A customizable framework for computing sky view factor from large-scale 3D city models, *Energy Build.* 149 (Supplement C) (Aug. 2017) 38–44.
- X. Li, C. Ratti, I. Seiferling, Quantifying the shade provision of street trees in urban landscape: a case study in Boston, USA, using google street view, *Landsc. Urban Plann.* 169 (Supplement C) (Jan. 2018) 81–91.
- J. Liang, et al., Automatic sky view factor estimation from street view photographs—a big data approach, *Rem. Sens.* 9 (5) (Apr. 2017) 411.
- R. Carrasco-Hernandez, A.R.D. Smedley, A.R. Webb, Using urban canyon geometries obtained from Google Street View for atmospheric studies: potential applications in the calculation of street level total shortwave irradiances, *Energy Build.* 86 (Supplement C) (Jan. 2015) 340–348.
- A. Middel, J. Lukaszczuk, R. Maciejewski, Sky view factors from synthetic fisheye photos for thermal comfort routing—a case study in Phoenix, Arizona, *Urban Plan.* 2 (1) (Mar. 2017) 19–30.
- E. Ng, C. Yuan, L. Chen, C. Ren, J.C.H. Fung, Improving the wind environment in high-density cities by understanding urban morphology and surface roughness: a study in Hong Kong, *Landsc. Urban Plann.* 101 (1) (May 2011) 59–74.
- Census and Statistics Department, The Government of Hong Kong S. A. R., “Population - Overview | Census and Statistics Department”, (2016) [Online]. Available: <http://www.censtatd.gov.hk/hkstat/sub/so20.jsp>, Accessed date: 25 October 2017.
- Planning Department, The Government of the Hong Kong, S. A. R., “Planning Department - Land Utilization in Hong Kong”, (2016) [Online]. Available: [http://www.pland.gov.hk/pland\\_en/info\\_serv/statistic/landu.html](http://www.pland.gov.hk/pland_en/info_serv/statistic/landu.html), Accessed date: 26 October 2017.
- Hong Kong Observatory, The Year’s Weather - 2016, (2016) [Online]. Available: <http://www.hko.gov.hk/wxinfo/pastwx/2016/ywx2016.htm>, Accessed date: 27 November 2017.
- E. Ng, V. Cheng, Urban human thermal comfort in hot and humid Hong Kong, *Energy Build.* 55 (Supplement C) (Dec. 2012) 51–65.
- W.-Z. Lu, H. He, A.Y.T. Leung, Assessing air quality in Hong Kong: a proposed,

- revised air pollution index (API), *Build. Environ.* 46 (12) (Dec. 2011) 2562–2569.
- [44] W. Wang, W. Zhou, E.Y.Y. Ng, Y. Xu, Urban heat islands in Hong Kong: statistical modeling and trend detection, *Nat. Hazards* 83 (2) (Sep. 2016) 885–907.
- [45] I.D. Stewart, T.R. Oke, Local climate zones for urban temperature studies, *Bull. Am. Meteorol. Soc.* 93 (12) (May 2012) 1879–1900.
- [46] Y. Zheng, et al., GIS-based mapping of Local Climate Zone in the high-density city of Hong Kong, *Urban Clim.* (Jun. 2017), <https://doi.org/10.1016/j.uclim.2017.05.008>.
- [47] Google Maps APIs, Google Street View Image API | Google Street View Image API, Google Developers, 2017 [Online]. Available: <https://developers.google.com/maps/documentation/streetview/intro>, Accessed date: 20 October 2017.
- [48] Google Maps APIs, Street View Image Metadata | Google Street View Image API, Google Developers, 2017 [Online]. Available: <https://developers.google.com/maps/documentation/streetview/metadata>, Accessed date: 27 November 2017.
- [49] H. Zhao, J. Shi, X. Qi, X. Wang, J. Jia, Pyramid scene parsing network, *ArXiv161201105 Cs* (Dec. 2016).
- [50] B. Zhou, H. Zhao, X. Puig, S. Fidler, A. Barriuso, A. Torralba, Semantic understanding of scenes through the ADE20K dataset, *ArXiv160805442 Cs* (Aug. 2016).
- [51] Y. LeCun, Y. Bengio, G. Hinton, Deep learning, *Nature* 521 (7553) (May 2015) nature14539.
- [52] V. Badrinarayanan, A. Kendall, R. Cipolla, SegNet: a deep convolutional encoder-decoder architecture for image segmentation, *ArXiv151100561 Cs* (Nov. 2015).
- [53] J. Long, E. Shelhamer, T. Darrell, Fully convolutional networks for semantic segmentation, Presented at the Proceedings of the IEEE Conference on Computer Vision and Pattern Recognition, 2015, pp. 3431–3440.
- [54] T.-Y. Lin, P. Dollár, R. Girshick, K. He, B. Hariharan, S. Belongie, Feature pyramid networks for object detection, *ArXiv161203144 Cs* (Dec. 2016).
- [55] MIT Senseable City Lab, Treepedia: MIT senseable city lab, Treepedia (2016) [Online]. Available: <http://senseable.mit.edu/treepedia>, Accessed date: 24 November 2017.
- [56] L. Chen, E. Ng, Quantitative urban climate mapping based on a geographical database: a simulation approach using Hong Kong as a case study, *Int. J. Appl. Earth Obs. Geoinformation* 13 (4) (Aug. 2011) 586–594.
- [57] C. Yuan, E. Ng, L.K. Norford, Improving air quality in high-density cities by understanding the relationship between air pollutant dispersion and urban morphologies, *Build. Environ.* 71 (Supplement C) (Jan. 2014) 245–258.
- [58] Y. Shi, K.K.-L. Lau, E. Ng, Developing street-level PM<sub>2.5</sub> and PM<sub>10</sub> land use regression models in high-density Hong Kong with urban morphological factors, *Environ. Sci. Technol.* 50 (15) (Aug. 2016) 8178–8187.
- [59] R. Giridharan, S.S.Y. Lau, S. Ganesan, B. Givoni, Urban design factors influencing heat island intensity in high-rise high-density environments of Hong Kong, *Build. Environ.* 42 (10) (Oct. 2007) 3669–3684.
- [60] C. Yuan, L. Chen, Mitigating urban heat island effects in high-density cities based on sky view factor and urban morphological understanding: a study of Hong Kong, *Archit. Sci. Rev.* 54 (4) (Nov. 2011) 305–315.
- [61] R. Ooka, T. Sato, K. Harayama, S. Murakami, Y. Kawamoto, Thermal energy balance analysis of the Tokyo metropolitan area using a mesoscale meteorological model incorporating an urban canopy model, *Bound.-Layer Meteorol.* 138 (1) (Jan. 2011) 77–97.
- [62] C.Y. Jim, Tree-canopy characteristics and urban development in Hong Kong, *Geogr. Rev.* 79 (2) (1989) 210–225.
- [63] F. Ali-Toudert, H. Mayer, Effects of asymmetry, galleries, overhanging façades and vegetation on thermal comfort in urban street canyons, *Sol. Energy* 81 (6) (Jun. 2007) 742–754.
- [64] J. Rodríguez-Algeciras, A. Tablada, A. Matzarakis, Effect of asymmetrical street canyons on pedestrian thermal comfort in warm-humid climate of Cuba, *Theor. Appl. Climatol.* (Jul. 2017) 1–17.
- [65] Google Street View, Google Street View – where We've Been & where We're Headed Next, Google Street View, 2017 [Online]. Available: <https://www.google.com/streetview/understand/>, Accessed date: 18 January 2018.